LAWRENCE
LIVERMORE
NATIONAL
LABORATORY

LLNL-CONF-609746

Event-by-Event Modeling of Prompt Neutrons and Photons from Neutron-Induced and Spontaneous Fission with FREYA

R. Vogt, J. Randrup

January 8, 2013

5th International Conference on "Fission and properties of neutron-rich nuclei"
Sanibel, FL, United States
November 5, 2012 through November 10, 2012

Disclaimer

Event-by-Event Modeling of Prompt Neutrons and Photons from Neutron-Induced and Spontaneous Fission with FREYA

R. VOGT*

Physics Division, Lawrence Livermore National Laboratory,
Livermore, CA 94551, USA
Physics Department, UC Davis, Davis, CA 95616, USA
**E-mail: vogt2@llnl.gov*

J. RANDRUP

Nuclear Science Division, Lawrence Berkeley National Laboratory
Berkeley, CA 94720, USA
E-mail: jrandrup@lbl.gov

The fast event-by-event fission code FREYA generates large samples of complete fission events. Using FREYA, it is possible to obtain the fission products as well as the prompt neutrons and photons emitted during the fission process, all with complete kinematic information. We can therefore extract any desired correlation observables. Concentrating on ^{239}Pu(n,f), ^{240}Pu(sf) and ^{252}Cf(sf), we compare our FREYA results with available data on prompt neutron and photon emission and present predictions for novel fission observables.

Keywords: fission, prompt neutron emission, prompt photon emission

1. Introduction

Phenomenological studies of nuclear fission are of particular interest for the detection of special nuclear material (SNM) for nonproliferation and security. Since all SNM emits neutrons and photons, studies of correlated emissions are especially interesting. In an event-by-event treatment, correlations between particles emitted during fission are automatically included.

The code FREYA (Fission Reaction Event Yield Algorithm).[1–3] simulates complete fission events with full kinematic information on the fission products and the emitted neutrons and photons. FREYA uses measured observables to improve our understanding of the fission process. Thus it is a potentially powerful tool for bridging the gap between current microscopic models and important fission observables as well as for improving estimates

of fission characteristics important for applications.

Here we first describe FREYA. We then show results for neutron and photon observables as well as associated correlations.

2. FREYA Inputs

We start with a fissile nucleus ${}^{A_0}Z_0$ with a specified excitation energy E_0^* and let it undergo binary fission into a heavy ${}^{A_H}Z_H$ and a light fragment ${}^{A_L}Z_L$. The fragment masses are obtained from experimental mass yields $Y(A)$ as explained in Ref.[2]

Once the mass and charge of the two fragments has been selected, the Q value of the fission channel is the difference between the total mass of A_0 and the fragment ground-state masses, $Q_{LH} = M(A_0) - M_L - M_H$. The Q_{LH} value is divided between the total kinetic energy (TKE) and the total excitation energy (TXE) of the fragments. The average TKE is assumed to take the form $\overline{\mathrm{TKE}}(A_H, E_\mathrm{n}) = \overline{\mathrm{TKE}}_\mathrm{data}(A_H) + d\mathrm{TKE}(E_\mathrm{n})$. The first term is extracted from data while the second is adjusted to the measured average neutron multiplicity, $\overline{\nu}$.

The fragments acquire angular momentum, $\boldsymbol{S}_f$ where $f = L, H$, at scission perpendicular to the line joining the fragment centers. The angular momentum components are sampled from a statistical distribution with temperature parameter T_S, $P(S_f^2) \sim \exp(-S_f^2/2\mathcal{I}_f T_S)$. where $\mathcal{I}_f$ is the moment of inertia of the fragment f. We employ half the rigid body value, $\mathcal{I}_f = \frac{1}{5} m_N r_0^2 A^{5/3}$. After the angular momenta are sampled, the rotational energy is $E_\mathrm{rot} = (\hbar^2/2)(S_L^2/\mathcal{I}_L + S_H^2/\mathcal{I}_H)$. The statistical fragment excitation energy is reduced correspondingly.

After the average total fragment kinetic energy, $\overline{\mathrm{TKE}}$, has been sampled, the combined statistical fragment excitation energy, $\overline{\mathrm{TXE}}$, follows from energy conservation, $\overline{\mathrm{TXE}} = \overline{E}_L^* + \overline{E}_H^* \doteq Q - \overline{\mathrm{TKE}} - E_\mathrm{rot}$. The first relation indicates that $\overline{\mathrm{TXE}}$ is partitioned between the two fragments.

If the fragments are in mutual thermal equilibrium, their temperatures are equal, $T_L = T_H$, and their statistical energy is proportional to the level-density parameter, *i.e.* $\overline{E}_f^* \sim a_f$. FREYA first assigns average excitations based on such equipartition, $\acute{E}_f^* = a_f(\tilde{E}_f^*)\overline{\mathrm{TXE}}/(a_L(\tilde{E}_L^*) + a_H(\tilde{E}_H^*))$. where $\tilde{E}_f^* = (A_f/A_0)\overline{\mathrm{TXE}}$. Subsequently, because the observed neutron multiplicities suggest that the light fragments are more excited (probably due to

The value of the asymptotic level density parameter, e_0, is obtained from the ^{239}Pu evaluation[3] and is assumed to be universal.

their greater distortion at scission), the average excitations are adjusted as $\overline{E}^*_L = x\acute{E}^*_L$, $\overline{E}^*_H = \overline{\mathrm{TKE}} - \overline{E}^*_L$, where $x > 1$ is a parameter.

After the mean excitation energies have been assigned, `FREYA` accounts for thermal fluctuations. The fragment temperature T_f is obtained from $\overline{U}_f \equiv U_f(\bar{E}^*_f) = a_f T_f^2$, where $U(E^*) = E^*$. The variance in the excitation E^*_f is then $\sigma_f^2 = 2\overline{U}^*_f T_f$. Therefore, for each of the two fragments, we sample a thermal fluctuation δE^*_f from a normal distribution of variance σ_f^2 and modify the fragment excitation energies as, $E^*_f = \overline{E}^*_f + \delta E^*_f$. Energy conservation causes a compensating fluctuation in TKE leading to TKE = $\overline{\mathrm{TKE}} - \delta E^*_L - \delta E^*_H$.[3]

Neutron evaporation occurs after the fragments have reached their asymptotic velocities. For a given fragment of statistical excitation E^*, the maximum temperature in its evaporation daughter, $T_{\max}$, is obtained from $aT^2_{\max} = E^* - S_n$, where S_n is the neutron separation energy. The neutron kinetic energy E is sampled from $f_n(E) \sim E\exp(-E/T_f^{\max})$. The emitted neutron is assumed to carry no angular momentum so the fragment angular momentum is unaffected by neutron emission. Neutrons are emitted as long as the Q value for emission exceeds $E_{n,\mathrm{cut}}$ where photon emission takes over.

After neutron evaporation has ceased, the residual product nucleus has a statistical excitation energy of $E^* < S_n + E_{n,\mathrm{cut}}$ and de-excites by sequential photon emission which occurs in two stages: first the statistical excitation energy is radiated away by sequential photon emission, leaving a cold but rotating product nucleus which then completes its de-excitation by photon emission along the yrast line.

Statistical photon emission is treated analogous to neutron evaporation except there is no separation energy for photons. Since the photons are massless, we introduce an infrared cut-off energy. Furthermore, there is an extra energy factor in the photon phase space, $f_\gamma(E) \sim E^2\exp(-E/T)$. Here T is the nuclear temperature prior to emission, equal to the maximum possible temperature after emission. Photons are emitted isotropically in the frame of the emitter nucleus. Emission continues until the available statistical excitation energy has been exhausted. The angular momentum is then disposed of by simulating a stretched E2 cascade for as long as $S > 2$. Each emitted photon emission reduces the angular momentum by two units and the energy by $E = (1/2)[S^2 - (S-2)^2]\hbar^2/\mathcal{I} = 2(S-1)\hbar^2/\mathcal{I}$. At the end of the cascade, when $S < 2$, a single final photon is emitted with the remaining excitation energy.

3. Neutron Results

We first present some neutron observables in Fig 1. The top right panel shows results for ^{252}Cf(sf) while the rest of the results are for ^{239}Pu(n,f).

The average neutron kinetic energy obtained from `FREYA` is compared to the Tsuchiya data[4] on ^{239}Pu(n,f) in the top left panel of Fig. 1. While the general trends are similar, `FREYA` somewhat overestimates the neutron kinetic energy near $A \approx 110$ and underestimates it near $A \approx 125$.

The top right panel of Fig. 1 presents measurements of ν(TKE) in ^{252}Cf(sf). The data with the steepest slope, by Bowman,[5] extracted TKE(A), but did not simultaneously measure the fragment yields. Thus the average neutron multiplicity depends only on TKE(A). Budtz-Jørgensen[6] measured both $Y(A)$ and TKE(A) so that ν(TKE) represents an average over both quantities. `FREYA` and `FIFRELIN`,[7] both shown with the data, also account for $Y(A)$ and TKE(A) and thus agree well with Budtz-Jørgensen[6] although `FREYA` reproduces the data somewhat better for TKE$>$ 200 MeV.

The bottom left panel of Fig. 1 compares the neutron multiplicity distribution $P(\nu)$ for ^{239}Pu(n,f) from `FREYA` to the compilation of Holden and Zucker.[8] Both results are considerably different from a Poisson because each neutron removes not only its kinetic energy but its separation energy while the Poisson only accounts for kinetic energy.

The observable $\nu(A)$ is very sensitive to the division of TXE between fragments, governed by the parameter x in `FREYA`. The characteristic 'saw-tooth' behavior is well reproduced by `FREYA`, as shown in the bottom right panel of Fig. 1. There is a minimum in $\nu(A)$ near $A_H \sim 132$, where TKE(A_H) is maximized.[11] Due to the closed shell at $A = 132$, the fragments are particularly resistant to neutron emission.

4. Neutron Correlations

We show the spectral shape for different values of ν and two-neutron correlations as a function of the angle between the neutrons in Fig. 2 for ^{240}Pu(sf), a contaminant of enriched ^{239}Pu, and ^{239}Pu(n,f) at $E_n = 0.5$ and 14 MeV. Comparing ^{240}Pu(sf) and ^{239}Pu($n_{\rm th}$,f) shows the difference between two systems with the same A_0 at similar excitation energies while the difference between $E_n = 0.5$ and 14 MeV shows the dependence on E_n.

The left-hand side shows the unit normalized spectral shape, $f_{\rm n}^{\nu}(E) \equiv (1/\nu)d\nu/dE$, for ν up to 6. The spectra become softer at higher ν because more neutrons share the available energy. This type of conservation-based correlation feature cannot be provided by "average" fission models. At $E_n =$

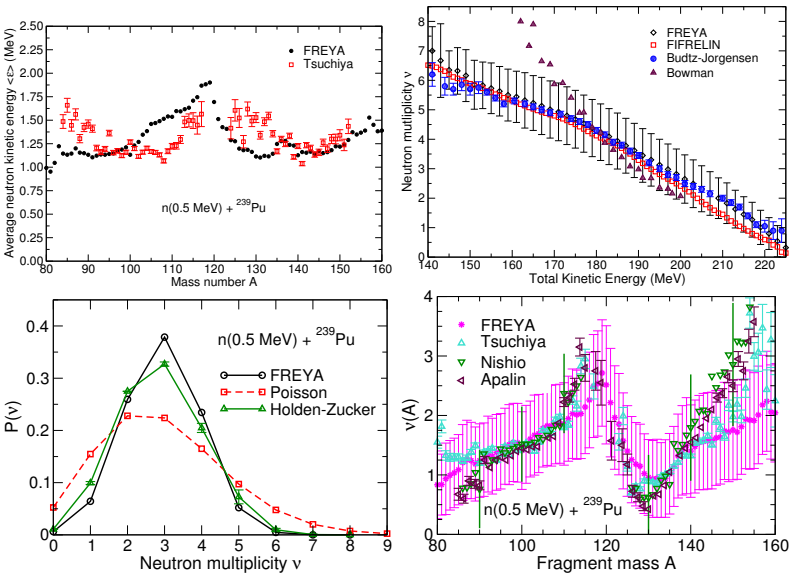

Fig. 1. (Top left) Average neutron kinetic energy for ^{239}Pu(n,f) from `FREYA` (•) compared to data[4] (□). (Top right) Average ν(TKE) measured by Budtz-Jørgensen[6] (•) and Bowman[5] (△) from ^{252}Cf(sf) compared to `FREYA` (◇), including the variance on ν(TKE), and `FIFRELIN`[7] (□). (Bottom left) Neutron multiplicity distribution, $P(\nu)$, for ^{239}Pu(n,f)[8] compared to `FREYA` (●) and a Poisson distribution (□). (Bottom right) Average $\nu(A)$ for ^{239}Pu(n,f). The `FREYA` results[11] (including variance) are compared to data from Tsuchiya[4] (△), Nishio[9] (▽), and Apalin[10] (◁).

14 MeV, there is a clear peak at $E_n - B_n \sim 8.4$ MeV at $\nu = 1$ due to pre-equilibrium emission. The high energy tail of the spectrum is all due to first-chance fission. As ν increases, the sharp peak is softened so that spectrum for $\overline{\nu}$ shows only a small change in slope.

The right-hand side of Fig. 2 shows the angular correlation between two neutrons with kinetic energies above $E = 0.5$, 1 and 1.5 MeV. The angular modulation at $\theta = 0$ grows more pronounced as the threshold is raised while the statistics are correspondingly reduced. The neutrons tend to be either forward or backward correlated. There is a significant correlation at $\theta_{12} = 0$ when both neutrons are emitted from the same fragment. The peak is higher in this case due to the higher velocity of the light fragment. The peak at $\theta_{12} = 180°$ arises because emission of one neutron from each fragment is most likely. The backward correlation is strongest when $\overline{\nu}$ is low, especially

The peak is at the highest available outgoing neutron energy.

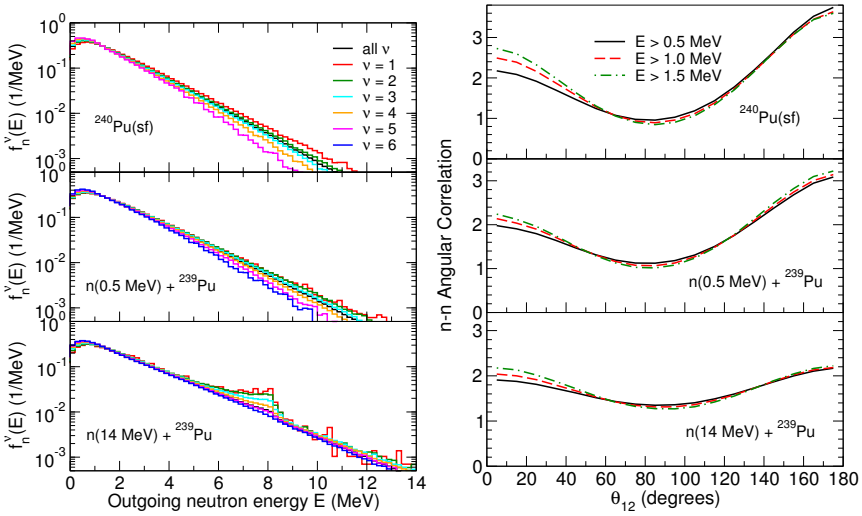

Fig. 2. (Top) The multiplicity-gated spectral distributions for neutrons emitted in association with fission of plutonium: ^{240}Pu(sf) (top), n(0.5 MeV)+^{239}Pu (middle), and n(14 MeV)+^{239}Pu (bottom), for specified neutron multiplicities $\nu = 1-6$ or any ν. (Right) The corresponding angular correlation between two neutrons with a minimum energy of either 0.5 MeV (solid), 1.0 MeV (dashed), or 1.5 MeV (dot-dashed).

for ^{240}Pu(sf)($\overline{\nu} \sim 2.15$). Large multiplicities reduce the correlation, see the difference between ^{239}Pu(n,f) at $E_n = 0.5$ and 14 MeV. At $E_n = 14$ MeV the emission pattern is nearly isotropic.

5. Photon Results

Finally, we present FREYA results compared to photon data spanning the last four decades, all taken on ^{252}Cf(sf). For further details, see Ref.[12]

The top left panel of Fig. 3 compares FREYA results on average total photon energy as a function of A, $E_\gamma(A)$, to data.[13] There is a sharp drop in the measured E_γ at symmetry, $A = 126$, while FREYA shows a dip near $A = 132$, similar to $\nu(A)$. While the statistics are rather poor, results for $T_S = 0.35$ and 0.75 MeV ($\overline{S}_f \sim 3.9\hbar$ and $5.8\hbar$ respectively) are, on average, too low to reproduce the data. The results for $T_S = 2.75$ ($\overline{S}_f \sim 11\hbar$) and $T_S = 0.2$ MeV ($\overline{S}_f \sim 3\hbar$ with $E_{n\,\mathrm{cut}} = 1$ MeV) are rather similar for the light fragment but differ for the heavy fragment.

The average photon energy decreases with TKE, as seen in the top right panel of Fig. 3. The Nardi data[13] starts out at lower $\overline{E}_\gamma$, becoming almost independent of TKE for TKE > 180 MeV. The FREYA result with

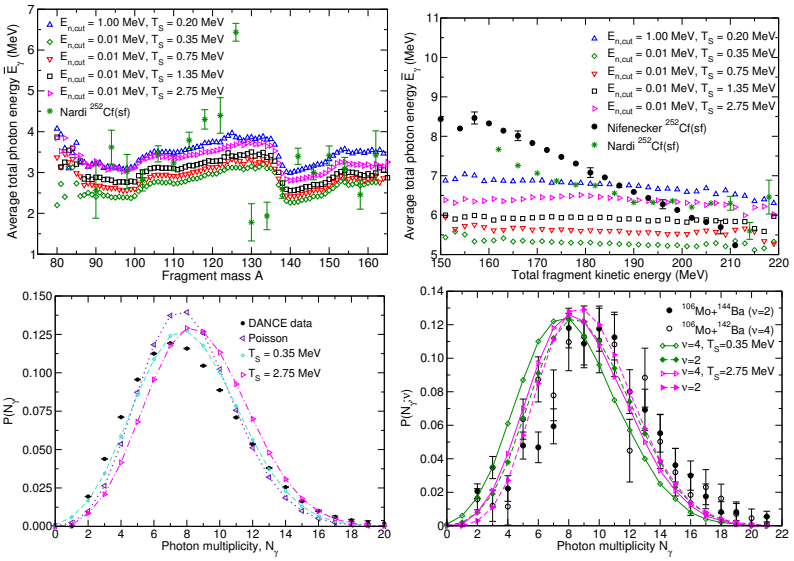

Fig. 3. Photon emission from ^{252}Cf(sf).[12] (Top left) The average total $E_\gamma(A)$ compared to data[13] ($*$)The calculations are $E_{n,\mathrm{cut}} = 1$ MeV, $T_S = 0.20$ MeV ($\triangle$) and, with $E_{n,\mathrm{cut}} = 0.01$ MeV, $T_S = 0.35$ ($\diamond$), 0.75 ($\bigtriangledown$), 1.35 ($\square$), and 2.75 MeV ($\triangleright$). (Top right) The average total E_γ(TKE) compared to data ($\bullet$)[14] and ($*$).[13] The calculations are $E_{n,\mathrm{cut}} = 1$ MeV, $T_S = 0.20$ MeV ($\triangle$) and, with $E_{n,\mathrm{cut}} = 0.01$ MeV, $T_S = 0.35$ ($\diamond$), 0.75 ($\bigtriangledown$), 1.35 ($\square$), and 2.75 MeV ($\triangleright$). (Bottom left) The photon multiplicity[15] ($\bullet$) compared to FREYA with $E_{n,\mathrm{cut}} = 0.01$ MeV and $T_S = 0.35$ ($\diamond$) and 2.75 ($\triangleright$) MeV as wellas Poisson with $T_S = 0.35$ MeV ($\triangleleft$). (Bottom right) The N_γ distribution gated on ν, averaged over all fragment masses, for $T_S = 0.35$ ($\diamond$) and 2.75 MeV ($\triangleright$). The solid curves with filled symbols show $\nu = 2$ while the dashed curves with open symbols show $\nu = 4$. The LiBerACE[16] Mo+Ba data with $\nu = 2$ ($\bullet$) and $\nu = 4$ ($\circ$) are also shown.

$E_{n,\mathrm{cut}} = 0.01$ MeV and $T_S = 2.75$ MeV is in relatively good agreement with this data at high TKE. The linear decrease of the Nifenecker data[14] with TKE agrees with neither the Nardi data nor FREYA. A new measurement of $\overline{E}_\gamma(A)$ and $\overline{E}_\gamma$(TKE) would be very helpful for resolving ssuch discrepancies in the data. Note also that the dependence of $\overline{E}_\gamma$(TKE) in FREYA is quite different than ν(TKE), as shown in the top right panel of Fig. 1.

The data of both Nardi[13] and Nifenecker,[14] while differing in detail, support a rather high value of fragment spin, $\sim 11\hbar$. However, the more recently DANCE photon multiplicity[15] is consistent with a lower value, $\overline{S}_f \sim 3.9\hbar$. Calculations with both $\overline{S}_f$ are compared to the data, along with the Poisson result, in the bottom left panel of Fig. 3. The resolution of the difference between the new and old data is important.

Finally, the LiBerACE data on neutron-photon correlations are com-

pared to FREYA calculations with $T_S = 0.35$ and 2.75 MeV in the bottom right portion of Fig. 3. Niefenecker claimed a strong positive neutron-photon correlation.[14] The LiBerACE data[16] instead show only a weak correlation. FREYA produces a slight anticorrelation, as might be expected from simple conservation laws. The lower value of T_S gives both a lower multiplicity and a stronger negative shift between $\nu = 2$ and $\nu = 4$ than the data.

6. Summary

The event-by-event nature of FREYA allows detailed studies of fission observables. FREYA agrees relatively well with most neutron observables, both for neutron-induced and spontaneous fission.[11] The existing photon data, on the other hand, do not present a very clear picture since they do not agree well with each other or some aspects of the newer data. FREYA does agree with the relatively large fragment spin suggested by the older experiments. However, there are still significant differences in detail.[12]

Acknowledgments

The work of R.V. was performed under the auspices of the U.S. Department of Energy by Lawrence Livermore National Laboratory under Contract DE-AC52-07NA27344. The work of J.R. was performed under the auspices of the U.S. Department of Energy by Lawrence Berkeley National Laboratory under Contract DE-AC02-05CH11231.

References

1. R. Vogt *et al.*, Phys. Rev. C **80**, 044611 (2009).
2. J. Randrup and R. Vogt, Phys. Rev. C **80**, 024601 (2009).
3. R. Vogt *et al.*, Phys. Rev. C **85**, 024608 (2012).
4. C. Tsuchiya *et al.*, J. Nucl. Sci. Technol. **37**, 941 (2000).
5. H. R. Bowman *et al.*, Phys. Rev. **129**, 2133 (1963).
6. C. Budtz-Jørgensen and H.-H. Knitter, Nucl. Phys. A **490**, 307 (1988).
7. O. Litaize and O. Serot, Phys. Rev. C **82**, 054616 (2010).
8. N. E. Holden and M. S. Zucker, BNL-NCS-35513 (1985).
9. K. Nishio *et al.*, J. Nucl. Sci. Technol. **32**, 404 (1995).
10. V. F Apalin *et al.*, Nucl. Phys. A **71**, 553 (1965).
11. R. Vogt and J. Randrup, Phys. Rev. C **84**, 044621 (2011).
12. R. Vogt and J. Randrup, submitted to Phys. Rev. C.
13. E. Nardi, A. Gavron and Z. Fraenkel, Phys. Rev. C **8**, 2293 (1973).
14. H. Nifenecker *et al.*, Nucl. Phys. A **189**, 285 (1972).
15. A. Chyzh *et al.*, Phys. Rev. C **85**, 02160(R) (2012).
16. D. L. Bleuel *et al.*, Nucl. Instr. Meth. A **624**, 691 (2010).